Overview of High Temperature Fibre Bragg Gratings and Potential Improvement Using Highly Doped Aluminosilicate Glass Optical Fibres

Maxime Cavillon, Matthieu Lancry, Bertrand Poumellec, Yitao Wang, John Canning, Kevin Cook, Thomas Hawkins, Peter Dragic, John Ballato

Overview of High Temperature Fibre Bragg Gratings and Potential Improvement Using Highly Doped Aluminosilicate Glass Optical Fibres

Maxime Cavillon[1,2], Matthieu Lancry[1], Bertrand Poumellec[1], Yitao Wang[1], John Canning[3], Kevin Cook[3], Thomas Hawkins[2], Peter Dragic[4], and John Ballato[2]

[1]Institut de Chimie Moléculaire et des Matériaux d'Orsay (ICMMO), Université Paris-Sud, Université Paris Saclay, CNRS, Orsay, France
[2]Center for Optical Materials Science and Engineering Technologies (COMSET) and the Department of Materials Science and Engineering, Clemson University, Clemson, SC, USA
[3]School of Electrical & Data Engineering, University of Technology Sydney, Australia
[4]Department of Electrical and Computer Engineering, University of Illinois at Urbana-Champaign, Urbana, IL, USA

E-mail: maxime.cavillon@u-psud.fr

Received xxxxxx
Accepted for publication xxxxxx
Published xxxxxx

Abstract

In this paper, various types of high temperature fibre Bragg gratings (FBGs) are reviewed, including recent results and advancements in the field. The main motivation of this review is to highlight the potential of fabricating thermally stable refractive index contrasts using femtosecond (fs) near-infrared (IR) radiation in fibres fabricated using non-conventional techniques, such as the Molten Core Method (MCM). As a demonstration to this, an yttrium aluminosilicate (YAS) core and pure silica cladding glass optical fibre is fabricated and investigated after being irradiated by fs laser within the Type II regime. The familiar formation of nanogratings inside both core and cladding regions are identified and studied using birefringence measurements and scanning electron microscopy (SEM). The thermal stability of the type II modifications is then investigated through isochronal annealing experiments (up to T = 1100°C; time steps, Δt = 30 min). For the YAS core composition, the measured birefringence does not decrease when tested up to 1000°C, while for the SiO_2 cladding and under the same conditions its value decreased by ~ 30%. These results suggest that inscription of such "*Type II fs-IR*" modifications in YAS fibres could be employed to make FBGs with high thermal stability. This opens the door toward the fabrication of a new range of "FBGs host fibres" suitable for ultra-high temperature operation.

Keywords: Fibre Bragg Gratings, High Temperature Sensing, Molten Core Method, Yttrium Aluminosilicates

1. Introduction

Over the past decade, research in the field of high temperature fibre Bragg gratings (FBGs) has continued at a steady pace, with a continuous increase of emerging applications. For example, such fibre technology is now employed in diverse areas such as temperature profiling of high~~t~~-temperature manufacturing equipment, [1], monitoring of fuel combustion machinery [2], temperature regulation of large diesel engines in trains [3], or to assess the structural integrity of a building post fire [4]. Oil and gas industries also benefit from such technology, as well as geothermal industries as they continue to drill ever-deeper into the earth, with exploration depths now reaching 5 km [5]. At these kind of depths the temperatures can exceed 500°C and extreme pressures are also encountered. In this paper, a short

introductory review of high and ultra-high temperature FBG sensors first is presented, following past reviews [6–8]. The prefixes "high" and "ultra-high" are defined herein for FBG operating temperature conditions below and above 800°C, respectively. This overview highlights the fact that the ultimate FBG thermal stability is closely linked to the intrinsic thermal stability of the core-cladding materials from which it is made. Therefore, the potential of unconventional fibre fabrication techniques, such as the Molten Core Method (MCM), for the fabrication of laser-induced structures with higher thermal resistance is discussed. As an example of this, a circular core/cladding glass fibre comprising a yttrium-doped aluminosilicate core (YAS) and a silica cladding is fabricated using the MCM. This system was chosen since a) aluminosilicate glasses such as YAS glasses are known to exhibit high glass transition temperatures (T_g ~ 900°C in Refs. [9,10]) and b) aluminosilicate and YAS glasses containing high Al_2O_3 concentrations typically present an increase in Al coordination number (4, 5, and 6 fold-coordination [11,12]), increasing glass network cross-linking density and bond strength. YAS glass core optical fibre is therefore expected to be a good glass candidate for high temperature applications.

The fibre core and cladding regions are subsequently irradiated by a femtosecond laser with varying laser parameters, such as laser pulse energy, and the laser-induced glass modifications are characterized through Retardance (R) measurements and scanning electron microscopy imaging. Retardance measurements enable the detection of birefringent structures, such as nanogratings (which are defined and discussed later), formed during laser irradiation.

Finally, a fibre segment is heat-treated up to 1100 °C and the thermal stability of the laser induced modifications in its core glass, compared to its silica cladding which serves as a reference, is investigated. Retardance measurements during these annealing experiments provide a direct mesurement of their thermal stability.

For completeness, if in the overview we principally discuss the various advancements in the field of FBGs operating at very high temperatures, it must be pointed out that other challenges are of prime importance. One of them is the necessity to find coatings, packaging and attachment procedures that can withstand such high temperature regimes. This includes the development of specialty coatings (silicone based coatings like polyimide up to 350°C (e.g., Refs. [13,14]) in continuous, metallic coatings like Al [15], Cu [16,17], Mo-Cu to 800°C [18], Au to 750°C [19], packaging in metallic capillaries like Inconel 600 [20] or steel to 1000°C [19]. Then one approach to attach these FBG sensors, especialy to metallic substrates, is to bond them using high temperature resistant adhesives. More sophisticated approaches may be to directly embed the FBGs into a metallic substrate thanks to additive layer manufacturing processes [21,22] or to use metal-coated FBGs and to braze them to the metallic structure. Athough of extreme importance, these topics are vast and go beyond the scope of this overview. An interested reader is directed to the aformentioned references for more information.

2. Types of fibre Bragg gratings (FBGs)

In this section, we discuss the different "types" of fabricated FBGs and their respective thermal stabilities. In this work, FBG "types" refer to the nature of refractive index modifications induced by laser irradiation rather than the growth kinetics, even if some types exhibit specific kinetics, such as Type I*n*. Type I corresponds to a laser irradiation regime that induces an isotropic increase of the refractive index. This is typically achieved by laser radiation (cw, ns, fs) that causes defect centers formation and glass densification [23,24]. The Type II regime relates to the formation of an anisotropic index change upon irradiation, typically induced by the presence of nanogratings, and results in the observation of form birefringence [25]. The laser-irradiated region has a lower refractive index than its surrounding (i.e., non-irradiated) medium. Finally, a type III regime corresponds to the formation of voids/microcavities (due to Coulombic micro-explosion) [26] usually using single pulse fs irradiation and likely accompanied by a densified shell [27].

2.1 Type I and Type In FBGs

Perhaps the most common kind of FBGs used for high-temperature operation are stabilized Type I FBGs. Generally, Type I gratings are stabilised to meet telecommunication specifications (-20°C ≤ T ≤ +80°C for time, t > 25 years) but can be processed to operate at much higher temperatures for short, but still usefull, timeframes depending on the application. For example, a Type I FBG can be thermally annealed at 700°C, reducing the FBG strength but allowing operation for finite time periods up to 600°C [28]. Other approaches to stabilize Type I gratings involve photosensitisation [29] to remove the unstable component generated during grating inscription.

Type I*n* FBGs, also called type IIA and negative index gratings [30], are formed in hydrogen-free silica fibres after a kind of regeneration [31–34]. This regeneration is thermally-induced through extended laser exposure times using, typically, quasi-continuous wave (CW), CW or pulsed UV lasers. Similar results may also be achieved through annealing in a furnace [35]. Type I*n* gratings form due to the relaxation of internal stresses that are induced from the UV radiation when the FBG is made, in particular the radial and axial stresses. The first Type I*n* FBGs were capable of operating up to T ~ 500°C before decaying [31,32]; however, by using higher intensity exposures, generating higher local

temperature, the functionallity may be extended to T ~ 700 – 800°C in step-index [33,34] and photonic crystal fibres [36]. Thermal properties strongly depend on the dopant nature (mostly Ge and B) and doping level, e.g. 1 hour at 500°C in highly (30 mole %) Ge-doped fibre; or 1 hour at 700°C in a Ge-B co-doped fibre [33,34].

2.2 Ultra-high temperature regenerated FBGs

In order to achieve FBG operation above 800°C in silica fibres the process of regeneration is required. Regenerated FBGs (RFBGs) are fabricated by annealing a so-called seed grating, typically (but not always) a Type I grating. Hydrogen is used to further increase strain in processed regions versus those that are unprocessed. The hydrogen can be added to the fibre prior to seed formation or later before the regeneration process. The ability to introduce hydrogen after the seed grating fabrication is key to making possible the regneration of draw tower gratings [37]. A seed grating is fabricated in a hydrogen-loaded silicate fibre using (typically but not always) a UV laser [38,39] and subsequently regenerated at temperatures in the range of T ~ 800 – 900°C. It is possible to also use femtosecond (fs) lasers to inscribe the seed [40]. Since these fibres are made of silica, these gratings can survive at T ~ 1295°C [41] or T ~ 1450°C for 20 to 30 minutes [42]. Regenerated gratings have also been demonstrated to continuously operate at T ~ 890°C for an impressive 9000 hours [43]. In contrast to thermal stabilization of Type I and Type I*n* FBGs, the high temperatures involved in the regeneration leads to the complete relaxation of stresses in the fibre. Regenerated gratings have, over the years, proven to be a viable sensing technology in a range of areas, for example in the profiling of high temperature manufacturing equipment [1], dual pressure/temperature sensing for gas turbines [44], sodium cooled nuclear reactors [20], high temperature air flow meters for internal combustion engines [45] and train engine temperature regulation [3]. Regenerated gratings have also been utilised to make the first accurate measurements of fibre viscosity [46]. Complex RFBG structures such as phase-shifted gratings [47], chirped gratings [48] and even final Bragg wavelength controlling [49] have been fabricated. Multiplexed distributed sensing also is possible [1,50].

Regenerated FBGs are commercially available (e.g., [19]). However, this comes along with few shortcomings: devices are limited to only few fibre compositions (e.g. regeneration efficiency is low in pure silica core fibres), the thermal engineering process leads to brittle fibres, mutiplexing FBGs in same fibres is possible [50] but difficult, and there is no available model to perform a reliable predition of long term operation.

2.3 Femtosecond FBGs (Type II and III FBGs)

Ultrafast lasers, typically in the near infrared (NIR) spectral range, are used to write FBGs (thereby known as femtosecond FBGs or fs-FBGs) either by using a phase mask [51] or by inscribing each grating plane point-by-point [52]. The use of visible or near infrared femtosecond laser light presents an inherent advantage of writing an FBG through the protective coating such as acrylate or polyimide [19]. Even if this coating does not withstand temperature beyond 350°C, it is particularly useful to get a preserved polymer coating for packaging and deployment issues. The use of NIR radiation means the excitation of the silica band edge is a multiphoton process and therefore highly localised, leading to much finer gratings than those achieved using two-photon absorption with 193 nm light [53,54]. Unlike the gratings inscribed using UV lasers, the mechanism responsible for index change does not necessarily depend on core chemical composition and does not require hydrogen. Gratings written using fs radiation may be classed as either being above or below the damage threshold of the glass. Because of the very high intensity fields achievable with these systems, highly localized plasma ionization and deoxygenation can lead to strong sub-diffraction interference effects between the plasma and the optical field, generating complex condensed structures such as nanogratings. These are based on glass decomposition that resolidifies into a nanoporous, usually silicon-rich structure, creating a strong and highly stable refractive index contrast [55]. Type I fs mostly are based on a glass fictive temperature T_f increase [56] when the duration of the heat pulse corresponding to the light energy is greater than the glass relaxation time $\eta(T)/G(T)$ (shear viscosity / shear modulus) with a partial contribution (typically 20%) of point defects [57]. However Type I fs-FBGs can be completely erased by annealing at temperatures exceeding 800°C. Type II gratings are attributed to the formation of self-organized nanogratings made of oxide decomposition [55]. Type II fs-FBGs demonstrate remarkable thermal stability up to ~ 1000°C for 150 hours after a stabilization for 1 hour at 1000°C [58], while operating for 100 hours at 1050°C reveals a slight (5%) intensity decay and a + 0.2 nm Bragg wavelength drift. This is likely associated with thermal relaxation of the bulk glass at these temperatures. As relates to applications, fs-FBGs have recently been tested as temperature sensors for monitoring fluidized bed combustors [2], as well as for radiation resistant temperature sensors [59]. Refractive index modifications are highly localized and involve significant stress-induced changes around the irradiated regions. For this reason, the higher temperature regime is limited by the thermal response of both the surrounding regions and the fibre itself which has not been relaxed prior to application. When the fibre is pre-annealed (before FBG writing) at high temperature (5 hours at 1100°C), Type II fs-IR FBGs are stable up to 1200°C during 20 hours [60]. Following this view, regeneration can also

improve fs-FBG performance to some extent [40,61]. In conventional single mode fibres (SMFs, Ge-doped silica glass), the point-to-point voids FBG (type III fs-FBGs) have slight loss of reflectivity (typically 20% of its initial strength) in less than 20 hours at 1000°C, before stabilizing [62]. At 1050°C, the reflectivity of point-by-point Bragg grating rapidly decreases to less than 20% after a few hours. Recently it was demonstrated that fs-FBGs fabricated via laser ablation in suspended-core microstructure fibre gratings can be operated at 1300°C for 5 minutes [63].

Types II and III femtosecond FBGs are now commercially available [64,65]. The main shortcomings are related to the lack of reliable lifetime prediction for long term operation above 800-1000°C where many processes occur, including not only residual stress relaxation of both the fibre and the laser-induced modifications, but also glass structural relaxation leading to changes of the glass disorder (fictive tempertaure changes).

2.4 Sapphire FBGs

To achieve even higher temperature operation FBGs can be inscribed in materials with higher melting points. Single crystalline aluminium oxide (sapphire) optical fibres have been used with femtosecond laser fabrication [66]. Sapphire FBGs demonstrate remarkable thermal stability up to ~ 1600°C for 6 hours after a stabilization for 20 minutes at 1745°C [67]. Sapphire FBGs boast the highest temperature performance to date, operable up to 1800°C. However, sapphire optical fibres presently are highly multimoded to their having an air cladding. Moreover, they are crystalline, leading to both short lengths and a lack of flexibility given their fairly large diameters. To date they are closer to thin rods than fibres. The next generation of fibres that may overcome this involves hybrid mixes of silica with aluminosilicate cores [68], provided their alumina concentration is sufficiently high to increase glass transition temperature.

Table 1 summarizes both maximum temperature of operation and wavelength shift as a function of temperature ($d\lambda/dT$) for the various types of gratings discussed above.

Table 1. Typical grating specifications for high temperature operation.

Grating type	Maximum temperature of operation (°C)	$d\lambda/dT$ (pm/°C)	Reference
Type I*n*	~700 (~1 h)	~12[a]	[33]
		12.8	[34]
Regenerated	~1295 (10 mins)	16.3	[39]
Femtosecond *Type II fs-IR*	~1000 (150 h)	~16[b]	[58]
Sapphire *fs - FBG*	~1600 (~6 h)	23.0 at room temperature	[66]
		31.0 at 1000 °C	
		31.0 at 1500 °C	

[a]: Estimated from figure 3 of Ref. [33].
[b]: Estimated from figure 4 of Ref. [58].

3. Molten core fabrication of high-temperature resistant structures

As seen from the previous overview, there is significant interest for waveguides and fibre sensors that can withstand high temperatures. Clearly, even if sapphire fibres/rods can withstand extremely high temperatures, they lack flexibility compared to a 125 μm cladding diameter conventional fibre, and are highly multimode. Unconventional techniques like the MCM, as opposed to conventional chemical vapor deposition (CVD) techniques, enable the fabrication of silicate glass optical fibres with high concentration of dopants (i.e., other than silica components) in their fibre cores. As an example of this, glass aluminosilicates with aluminium oxide (or alumina) concentrations as high as $[Al_2O_3]$ ~ 55 mole % at the core center were fabricated using this technique [69]. Subsequent to this, FBGs with varying content of alumina (4% and 30% [70], and 50% [68]) have been successfully fabricated. For the highest fibre concentration ($[Al_2O_3]$ = 50 mole %), good thermal stability up to 1000°C was reported.

3.1 Experimental procedure

The fibre investigated in this study, which is refered as "YAG-derived fibre," was fabricated using the molten core method. More details regarding the fabrication process can be found in Ref. [71]. In short, a rod-shaped yttrium aluminium garnet (YAG) crystal of 2.75 mm diameter and 60 mm length was inserted inside a F300 pure silica glass capillary tube (3 mm and 30 mm inner and outer diameters, respectively). The ensemble was placed inside a high temperature graphite furnace and brought to T ~ 2000°C. At this temperature, the YAG precursor melts, and silica from the capillary tube preform partially is dissolved into the precursor molten core, yielding a SiO_2-Y_2O_3-Al_2O_3 (yttrium aluminosilicate, YAS) core glass. The preform is subsequently drawn into an optical fibre with a targeted cladding diameter of 125 μm, and a conventional acrylate polymer coating was deposited on-line during the draw. A total fibre length of ~800 m was collected, and a few meters were selected for this work. In Figure 1a the compound concentration profile across the fibre core is displayed.

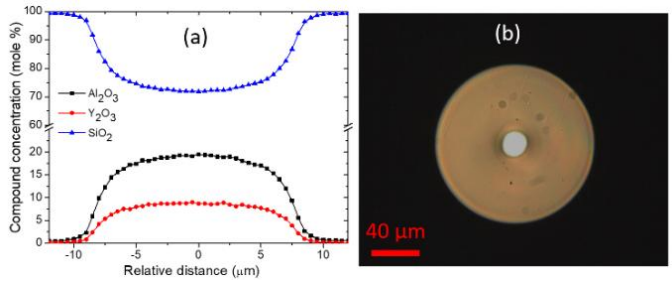

Figure 1. a) Concentration profile of the fibre core composition and b) optical microscope (bottom light illumination) image of the fibre cross section.

Figure 1b shows the fibre cross section under an optical microscope. The fibre core concentration profile was measured by Energy Dispersive X-ray (EDX) with a ZEISS SUPRA 55 VP Scanning Electron Microscope (SEM). Additional information regarding specific fibre properties for these YAG-derived fibres fabricated using the MCM can be found in Refs. [72,73]. Typical background losses at 1.55 μm and numerical aperture values in these fibre systems are ~0.5 dB/m and ~0.5, respectively. However, these values can be adjusted depending on the precursor purity used (for losses) and the amount of dopants incorporated into the core (for numerical aperture). For completeness, it is worth mentioning that these fibre segments can easily be spliced to conventional single mode fibres.

The refractive index profile (RIP) measurement of the glass fibre was performed at 550 nm with an IFA-100 Multiwavelength Optical Fibre Analyzer (Interfiber Analysis). The refractive index at the fibre core center will be used for calculations to determine glass properties in next section (Section 3.2). Femtosecond laser irradiation (λ = 1030 nm) was performed on the YAG-derived fibre, in both core and cladding regions. In order to irradiate the fibres, each selected fibre segment (□5 cm length) had its coating removed, then was sandwiched between a fused silica glass slide (bottom) and a borosilicate glass cover-slip (top, ~170 μm thin), with some index matching oil (GN Nettest, n_D=1.4580 at 25°C) in between. Additionally, to ensure the fibre segments were properly affixed to the substrate during the heat-treatment analysis described below, both ends of each segment were adhered to the bottom silica substract using high temperature adhesive. Finally, the ensemble was placed on a translation stage, carefully aligned with respect to the fs laser beam, then irradiated. More information regarding the laser setup can be found in Ref. [74].

Following a geometry similar to line-by-line FBG writing, a first experiment consisted in drawing 60 μm lines, perpendicular to the direction of fibre longitudinal axis, enabling irradiation in both core and cladding, as shown in Figure 2a. The spacing between each line is 5 μm, and the pulse energy varies by step of 0.1 μJ, ranging from 0.1 to 1.0 μJ. Other lasers parameters are: 1030 nm laser wavelength, 100 kHz laser pulse repetition rate; 100 μm/s speed (resulting in a pulse overlap rate of 1000 pulses/μm); NA (writing objective) = 0.6; and laser polarization perpendicular (⊥) or parallel (//) to the writing direction (Figure 2a). The retardance (R, in nm) of the irradiated regions was mesured at room temperature, using the Senarmont compensator technique on a Olympus BX51 optical microscope. R is defined as R=B×d, with B being the linear birefringence (dimensionless) and d the thickness of the birefringent object (in nm). Hence, when a fibre segment is irradiated by a laser and a birefringent object is formed, the measured R value corresponds to the amount of B integrated over the laser track length (in the z direction from Figure 2). For completeness, the fibre segment is immersed in the index matching oil for each Retardance measurement, which removes curvature effects from circular fibre geometry during analysis.

A second experiment was performed to investigate the morphology of fs laser induced glass modifications in the YAG-derived fibre (both in core and cladding). In this experiment, a total of 6 lines of 10 mm lengths (5 μm interval between them) parallel to the light propagation axis of the fibre were irradiated, as represented in Figure 2b. The pulse energy was set to 0.8 μJ/pulse, based on the previous set of experiments, found to be within the type II regime. Next, the fibre segment was cleaved and the fibre cross sectional area was investigated using a Scanning Electron Microscope (SEM, Field-Emission Gun Scanning Electron Microscope, ZEISS SUPRA 55 VP, 1 kV accelerating voltage). This experiment was repeated using two different laser polarization orientations: parallel (//) and perpendicular (⊥) to the laser writing inscription. The former condition enables the observation of the inside (which are porous in bulk SiO_2 [55]) of the laser-induced nanoplanes, while the latter permits sideways visualization of these nanoplanes, including their spacing [74].

Finally, a fibre segment was irradiated according to Figure 2a and was subsequently heat-treated up to 1100°C by incremental temperature steps (400°C, 500°C, 600°C, 700°C, 800°C, 850°C, 900°C, 950°C, 1000°C, 1050°C, 1075°C, and 1100°C) and with a constant heat-treament time (30 minutes) for each temperature step. R was measured at room temperature between each isochronal annealing step.

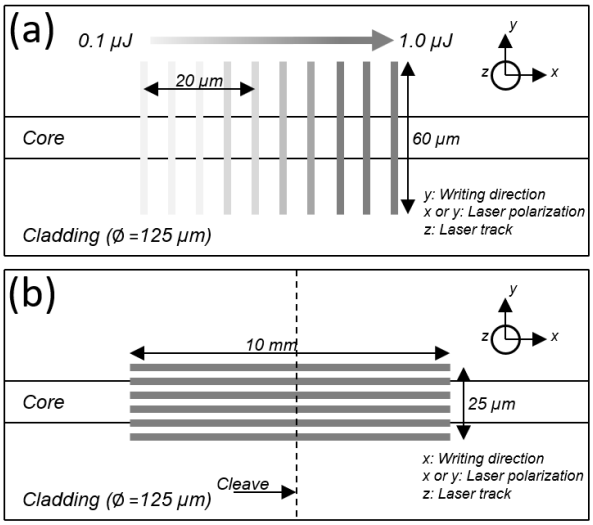

Figure 2. Experimental laser writing designs. a) Irradiation of fs laser inside fibre core and cladding of an optical fibre at different pulse energies (λ = 1030 nm, 100 kHz, 100 µm/s, 10^3 pulses/µm, NA = 0.6, pulse duration = 160 fs). b) Longitudinal (along x) irradiation at constant pulse energy (0.8 µJ) using different laser polarization conditions: parallel (//, along x) and perpendicular (⊥, along y) to the writing direction.

3.2 Experimental results

3.2.1 Laser irradiation

Measurements of retardance (R) as a function pulse energy and under different polarization (⊥ and //) conditions are shown in Figure 3, for both SiO_2 (taken in the fibre cladding) and the YAS glass core, taken at the core center.

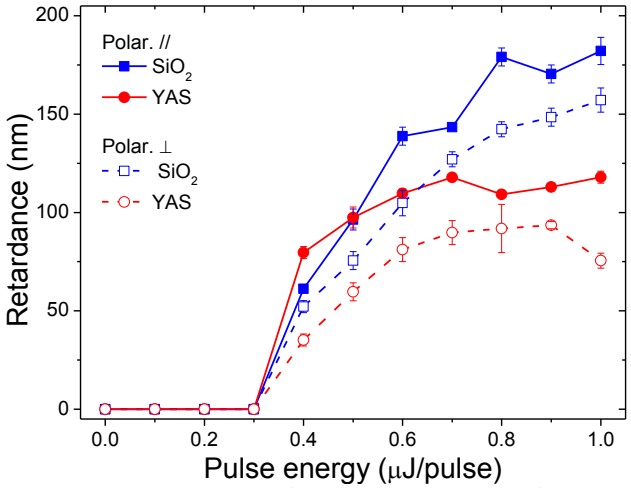

Figure 3. Retardance (R) as a function of pulse energy for: YAG-derived fibre both at the core center (YAS, in red) and in its cladding (silica, in blue). Experimental conditions are: λ = 1030 nm, 100 kHz, 100 µm/s, 10^3 pulses/µm, NA = 0.6, pulse duration = 160 fs, laser polarization ⊥ and // to writing direction.

Both the YAS and SiO_2 glasses exhibit a very similar behavior, that is, a threshold situated at 0.35 ± 0.025 µJ, above which a strong retardance appears whose slow axis is set by the laser polarization. This is characteristic of the formation of nanogratings in silica [56,74], and is associated with a local decrease of refractive index within the irradiated region. For the YAS composition, R appears to plateau above 0.6 µJ/pulse, and its overall magnitude is lower than for SiO_2. R values are lower for ⊥ configuration relative to // configuration. Such polarization dependence is explained by the boundary conditions [75] and spatial-temporal properties of the ultrashort pulse laser beam quantified by the pulse front tilt leading to anisotropic photosensitivity phenomena [76].

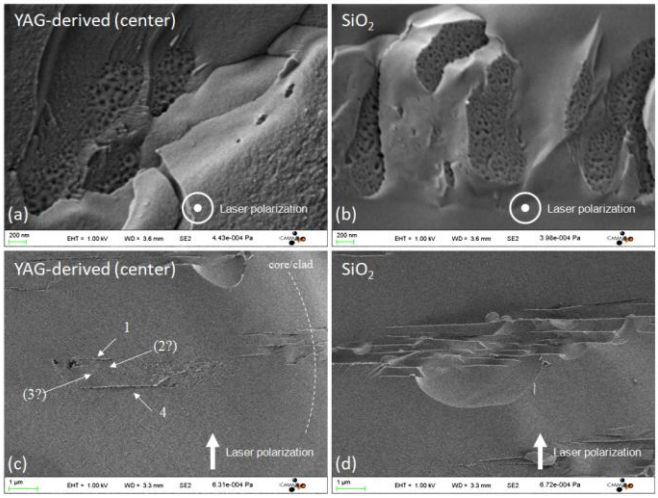

Figure 4. Scanning electron micrographs in the YAG-derived fibre, both at the core center (YAS) and in the cladding (SiO_2), for parallel (a & b) and orthogonal (c & d) laser polarization direction with respect to the writing direction. // configuration enables observation of the inside of the nanogratings revealing their nanoporosity (a & b), while ⊥ configuration permits sideways visualization of the nanogratings. Laser parameters: λ = 1030 nm, 100 kHz, 100 µm/s, 10^3 pulses/µm, NA = 0.6, pulse duration = 160 fs, E=0.8 µJ/pulse.

To better understand the dissimilarities observed from Figure 3 between the YAG-derived YAS glass core and the silica cladding, an electron micrograph analysis is carried out as described in Section 3.1. In Figure 4, SEM micrographs of the fibre cross sections with the laser polarization direction either // (Figures 4a and 4b) or ⊥ (Figures 4c and 4d) to the writing direction are reported. First, from Figures 4a and 4b, the formation of porous nanogratings is clearly identified in both cladding (silica) and core (YAS) regions, which demonstrates the feasibility of inscribing nanogratings inside this glass composition family (within the range of compositions and laser parameters studied herein). Second, by comparing Figure 4c with Figure 4d, one can observe that at core center a less dense network of nanoplanes are visible compared to the irradiated pure silica cladding region. If only two nanoplanes are easily identified (labeled as 1 and 4 in Figure 4c), two other ones (labeled as "2?" and "3?") seem to be on the verge of formation. This is in agreement with the reduction of the interplanar distance when increasing pulse numbers in SiO_2 [77].

Table 2. Comparison between typical nanoplanes' parameters for the YAG-derived fibre at both core center (YAS) and in the cladding (SiO_2).

Materials	SiO_2	YAS
Porosity filling factor, ff. (%)	41,3 ± 0.9	44,5 ± 2.6
Period of the nanoplanes, Λ (nm)	330 ± 7	□1015 or □338[d]
Thickness of porous layer, δ (nm)	42.2 ± 5.5	61.2 ± 11
Laser track length, d (μm)	19,95 ± 1.0	□13,5
Measured Retardance, R (nm) (at 551 nm)	142 ± 3.8	92 ± 12.2
Index glass background, n_{BG} (550 nm)	1,4599	1,5559[a]
Index porous regions[b], n_{PR} (550 nm)	1,269	1,308
Birefringence, B ($\|n_e-n_o\|$)[c]	□6.3×10^{-3}	□5.3×10^{-3}
Calculated retardance, R_c (nm)[c]	~125	~71[e]

[a]*: Determined from Refractive Index Profile.*
[b]*: Calculated using the Maxwell-Garnett approximation (Equation 18 in Ref.* [78]*).*
[c]*:* $n_0 = \{[(\Lambda-\delta)/\Lambda]\times n_{BG}^2 + [\delta/\Lambda]\times n_{PR}^2]\}^{1/2}$, $n_e = \{[(\Lambda/(\Lambda-\delta)]\times n_{BG}^2 + [\Lambda/\delta]\times n_{PR}^2]\}^{1/2}$*, in Refs.* [74,79]*, and* $R_c = B\times d$.
[d]*: In Figure 4 only two planes are clearly visible in the magnified region. However, the reader should be informed that two additional planes "in formation" have been identified between the already existing two, which would bring the nanograting periodicity to □338 nm.*
[e]*: Calculated with* $\Lambda = 1015$ *nm.*

Based on the results of Figures 3 and 4, it can be stated that the increase of R for YAG-derived YAS glass fibre core is expected to be of the same origin as for SiO_2, i.e., formation of a periodic array of porous nanoplanes separated by non-porous glass [55], cooperating to form birefringence [25] . The various parameters that factor into the total R value are identified, measured, and summarized in Table 2, and more details can be found in Ref. [74]. The porosity filling factor (ff), which account for the volume of pores per unit glass volume, is found to be slightly higher at the core center than in the silica cladding, while the thickness of its nanoplanes is consequently higher (□45% increase). Now looking at the nanoplane periodicity (Λ), at first, it appears that it is much larger at the core center if we only consider the two well-formed planes (1015 nm versus 330 nm for silica). However, if 4 planes are considered, which includes planes 1, 2, 3, and 4 from Figure 4c, then Λ = 338 nm, which is close to the value for silica.

Finally, the laser track length (d) is found to be shorter at the core center than in the cladding (13.5 μm versus 19.95 μm). Since d is known and the Birefringence can be calculated based on the parameters in Table 2 (see Ref. [74] for more details), R can be calculated as well (R=B×d) for both cladding and core laser tracks. In the latter case, the nanoplanes throughout the laser track are assumed identical to those at the very core center (i.e., having the same properties), which is certainly not true in reality as the fibre has a graded index profile associated with its composition gradient (see Figure 1). However, this assumption is made as the aim of this calculation is to provide a semi-quantitative calculation of what R value can be expected when parameters in Table 2 are employed. The calculated R values (R_c) for cladding and core materials were □125 nm and □71 nm, respectively. These values are in fairly good agreement with the measured values (□142 nm and □72 nm, respectively), although a bit lower in magnitude for SiO_2. This can be attributed to the stress field contribution associated with the formed nanoplanes [80]. Moreover, it appears that the R values between core and cladding principally differ due to their different laser track lengths, but the calculated form birefringence values from the nanostructures opto-geometrical parameters (see Table 2) are somewhat similar (□6.3×10^{-3} in SiO_2 versus □5.3×10^{-3} in YAS).

3.2.2. Thermal stability

The YAG-derived fibre segment was heat-treated to 1100°C after inscription following Figure 2a. R as a function of temperature, R(T), was measured for each energy. The R(T) profile was found to be independent of the pulse energy, although its magnitude is changed (lower pulse energy results in lower R values, as shown in Figure 3). Consequently to this, for each temperature the retardance was averaged over the whole energy range investigated (from 0.1 μJ to 1 μJ). The latter was thus normalized relative to its initial (at T = 25°C) value, and this operation was repeated for SiO_2 and YAS both in // and ⊥ writing conditions. The results are displayed in Figure 5.

From Figure 5, the evolution of R as a function of temperature shows some characteristic features, commonly found in both the YAG-derived fibre core center and cladding. First, there is a slight increase in the R value up to 700°C, more pronounced for both the core center and the SMF samples. Such a feature is attributed to the annealing of point defects formed mostly within nanoplanes [79], promoting an increase of nanogratings index contrast, thus B and, in our case, R. From Ref. [81], defects such as non-bridging oxygen hole-centers (NBOHC) relax between 300°C – 600°C, and this within a few minutes at 600°C. This also is the case for SiE' defects. In other words, this is attribued in the literature to the co-existence of both Type I and Type II index changes [82]. In contrast, changes in Si-O three and four-fold rings anneal out at higher temperatures (typically 700 °C – 900 °C range) [81].

As the heat-treatment temperature is increased, induced stress relaxes and consequently to this the refractive index contrast further lessens, and so does R. Finally, above 1000°C, R diminishes dramatically, and no birefringence is detected after 1075°C (and the laser tracks are not visible under optical microscope). Beyond 1100°C both glasses (YAS and SiO_2) converge to R=0.

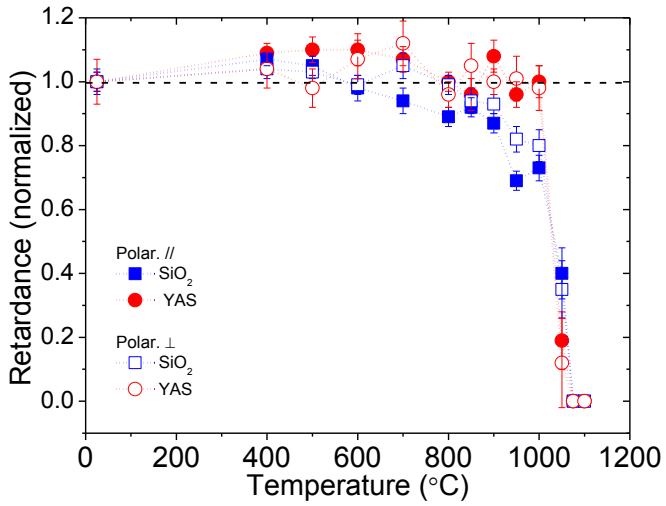

Figure 5. Normalized retardance (averaged over the 0.1 to 1.0 µJ pulse energy range) as a function of temperature for YAG-derived fibre at the core center (YAS) and in the cladding (SiO_2), for both // and ⊥ configurations. The measurements were performed at room temperature.

By comparing thermal behavior for both SiO_2 and YAS glasses, the former (SiO_2) exhibits a decrease in R values starting roughly around 700 °C. On the other hand, the latter (YAS) shows no decrease in R up to 1000 °C. At this temperature, R value for SiO_2 has already decreased by ~30%, and suggests that femtosecond-written nanogratings (or so called type II regime) in YAG-derived fibres may present advantages for high temperature operations over conventional silicate-based fibres. In particular it should be noted that pure silica core fibres have a F-doped cladding, whereas common fibres like SMF-28 have a Ge-doped core, which impacts the high temperature performances of such FBGs.

4. Conclusions

An overview of FBGs for high and ultra-high temperature applications was presented and, in particular, the ability of Type II and Type III femtosecond-laser induced nanostructures to withstand ultra-high temperatures was discussed.

Here, femtosecond-inscription on a yttrium aluminosilicate core – silica cladding glass optical fibre was investigated. It was shown that Type II (nanograting structures) can be photo-induced in this glass composition, and that the laser parameters investigated (pulse energy range, polarization orientation) show that the yttrium aluminosilicate core material response to fs laser irradiation globally resembles that of SiO_2. Additionally, isochronal thermal annealing show an improved thermal stability of Type-II modifications written in the core material compared to its SiO_2 cladding. Indeed, the measured retardance in the core shows no decrease in magnitude at temperatures lower than 1000°C. In contrast, in the F300 SiO_2 cladding, the retardance lowers after 700°C – 800°C, and has already decreased by ~30% at 1000°C. Fabrication of fibres with lower SiO_2 concentration in the core—(i.e., higher Y_2O_3 and Al_2O_3 dopant concentration) may permit fabrication of fs-laser structures with even higher thermal stability. Further work is underway to characterize nanogratings inscribed in fibre core segments with higher Y_2O_3 and Al_2O_3 content, as well as writing FBGs in these fibre families for lifetime prediction analysis.

Finally, in this paper the Authors advocate an approach based on the development of new fibres with high melting points conjugated to femtosecond direct writing. In this view, a proposal to the development of such fibres would be possible through the use of nonconventional fibre fabrication techniques, such as the molten core method (MCM). These "high temperature fibres" could be composed of aluminosilicate cores such as Al_2O_3-SiO_2 (>50 mole% of Al_2O_3), Y_2O_3-Al_2O_3-SiO_2 (as reported in this paper) and potentially fibres with other compositions like in binary SiO_2-ZrO_2 or ternary SiO_2-ZrO_2-Al_2O_3 glass systems. This fibre fabrication method to develop a new range of host fibres suitable for writing ultra-high temperature FBGs and overcoming the current performances of pure silica core or Ge-doped SiO_2 fibres appears promising.

Acknowledgements

The Authors would like to acknowledge Francois Brisset (ICMMO, Université Paris-Sud) for his support in electron microscopy. The Author's (JB and PD) acknowledge financial support from the US Department of Defense High Energy Laser Joint Technology Office (HEL JTO). ML and BP would like to thank CNRS Défi Instrumention aux limites – UltraBragg – for financing this work.

References

[1] Åslund M L, Canning J, Canagasabey A, Assis de Oliveira R, Liu Y, Cook K and Peng G 2012 Mapping the thermal distribution within a silica preform tube using regenerated fibre Bragg gratings *Int. J. Heat Mass Transf.* **55** 3288–94

[2] Walker R B, Ding H, Coulas D, Grobnic D, Mihailov S J, Duchesne M A, Hughes R W, McCalden D J and Burchat R 2015 Entrained-flow gasifier and fluidized-bed combustor temperature monitoring using arrays of fs-IR written fiber Bragg gratings *24th International Conference in Optical Fibre Sensors (OFS24)* p 96343X

[3] Mezzadri F, Janzen F C, Martelli C, Canning J and Cook K 2012 Monitoramento de temperatura em turbina de motor diesel de locomotiva com sensor a fibra optica *15th Brazilian Symposium for Microwaves and Optoelectronics (SBMO) and the 10th Brazilian Congress for Electromagnetics (CBMag)*

[4] Rinaudo P, Torres B, Paya-Zaforteza I, Calderón P A and Sales S 2015 Evaluation of new regenerated fiber Bragg grating high-temperature sensors in an ISO 834 fire test *Fire Saf. J.* **71** 332–9

[5] Unnikrishnan K 2017 Iceland is drilling the world's deepest geothermal well *Digit. J.*

[6] Canning J, Stevenson M, Cook K, Aslund A, Ecke W,

Willsch R, Bartelt H, Kalinowski H J, Grabarski L, Oliveira V, Martelli C, Braga A, Groothoff N and Peng G-D 2009 Optical fibre Bragg gratings for high temperature sensing *20th International Conference on Optical Fibre Sensors* p 75032N

[7] Mihailov S J, Grobnic D, Hnatovsky C, Walker R B, Lu P, Coulas D and Ding H 2017 Extreme Environment Sensing Using Femtosecond Laser-Inscribed Fiber Bragg Gratings *Sensors* **17**

[8] Liao C R and Wang D N 2013 Review of femtosecond laser fabricated fiber Bragg gratings for high temperature sensing *Photonic Sensors* **3** 97–101

[9] Johnson J, Weber R and Grimsditch M 2005 Thermal and mechanical properties of rare earth aluminate and low-silica aluminosilicate optical glasses *J. Non. Cryst. Solids* **351** 650–5

[10] Lago D C and Prado M O 2013 Crystallization of yttrium and samarium aluminosilicate glasses *Phys. Procedia* **48** 10–6

[11] Weber R, Sen S, Youngman R E, Hart R T and Benmore C J 2008 Structure of high alumina content Al_2O_3-SiO_2 composition glasses *J. Phys. Chem. B* **112** 16726–33

[12] Schaller T and Stebbins J F 1998 The Structural Role of Lanthanum and Yttrium in Aluminosilicate Glasses: A ^{27}Al and ^{17}O MAS NMR Study *J. Phys. Chem. B* **102** 10690–7

[13] Betz D, Trutzel M N, Staudigel L, Martin W and Krumpholz O 2000 Fiberoptic Smart Sensing of Component Deformations in Adaptive Wings *ICAS 2000 Congress* pp 495.1-495.10

[14] Huang L, Dyer R S, Lago R J, Stolov A A and Li J 2016 Mechanical properties of polyimide coated optical fibers at elevated temperatures *Optical Fibers and Sensors for Medical Diagnostics and Treatment Applications XVI* vol 9702 p 97020Y

[15] Semjonov S L, Bubnov M M, Dianov E M and Shchebunyaev A G 1994 Reliability of aluminum-coated fibers at high temperature *Proc. SPIE 2074, Fiber Optics Reliability and Testing: Benign and Adverse Environments* ed D K Paul and H H Yuce

[16] Biriukov A S, Bogatyrjov V A, Lebedev V F, Sysolyatin A A and Khitun A G 1998 Strength and Reliability of Metal-Coated Optical Fibers at High Temperatures *MRS Proc.* vol 531 pp 297–300

[17] Stanczyk T, Fidelus J, Wysokinski K, Lipinski S, Tenderenda T, Kuklińska M, Kołakowska A, Rodriguez Garcia J, Canadas Martinez I and Nasiłowski T 2015 Influence of high temperatures on optical fibers coated with multilayer protective coatings *Proc. SPIE 9816, Optical Fibers and Their Applications 2015* p 98160F

[18] He J, Ding L, Cai J, Zhu W and Dai J 2019 A novel high temperature resistant Mo-Cu functional gradient coating for optic fiber Bragg grating *Results Phys.* **14** 102456(2-10)

[19] Technica *https://technicasa.com/*

[20] Laffont G, Cotillard R, Roussel N, Desmarchelier R and Rougeault S 2018 Temperature resistant fiber bragg gratings for on-line and structural health monitoring of the next-generation of nuclear reactors *Sensors* **18**

[21] Jinesh M, MacPherson W N, Hand D P and Maier R R J 2016 Stainless steel component with compressed fiber Bragg grating for high temperature sensing applications *Proc. SPIE 9916, Sixth European Workshop on Optical Fibre Sensors* p 99160J

[22] Tu Y, Ye L, Zhou S P and Tu S T 2017 An improved metal-packaged strain sensor based on a regenerated fiber bragg grating in hydrogen-loaded boron–germanium co-doped photosensitive fiber for high-temperature applications *Sensors* **17** 1–18

[23] Kashyap R 2010 *Fiber Bragg Gratings* (Academic Press, Elsevier)

[24] Chan J W, Huser T, Risbud S and Krol D M 2001 Structural changes in fused silica after exposure to focused femtosecond laser pulses *Opt. Lett.* **26** 1726–8

[25] Bricchi E, Klappauf B G and Kazansky P G 2004 Form birefringence and negative index change created by femtosecond direct writing in transparent materials *Opt. Lett.* **29** 119–21

[26] Glezer E N, Milosavljevic M, Huang L, Finlay R J, Her T-H, Callan J P and Mazur E 1996 3-D Optical Storage Inside Transparent Materials *Opt. Lett.* **21** 2023–6

[27] Martinez A, Dubov M, Khrushchev I and Bennion I 2006 Photoinduced Modifications in Fiber Gratings Inscribed Directly by Infrared Femtosecond Irradiation *IEEE Photonics Technol. Lett.* **18** 2266–8

[28] Åslund M L, Canning J, Stevenson M and Cook K 2010 Thermal stabilization of Type I fiber Bragg gratings for operation up to 600 °C *Opt. Lett.* **35** 586–8

[29] Canning J 2000 Photosensitization and Photostabilization of Laser-Induced Index Changes in Optical Fibers *Opt. Fiber Technol.* **6** 275–89

[30] Canning J 2008 Fibre gratings and devices for sensors and Lasers *Laser Photonics Rev.* **2** 275–89

[31] Dong L and Liu W F 1997 Thermal decay of fiber Bragg gratings of positive and negative index changes formed at 193 nm in a boron-codoped germanosilicate fiber *Appl. Opt.* **36** 8222–6

[32] Dong L, Liu W F and Reekie L 1996 Negative-index gratings formed by a 193-nm excimer laser *Opt. Lett.* **21** 2032–4

[33] Groothoff N and Canning J 2004 Enhanced type IIA gratings for high-temperature operation *Opt. Lett.* **29** 2360–2

[34] Frazão O, Lima M J N and Santos J L 2003 Simultaneous measurement of strain and temperature using type I and type IIA fibre Bragg gratings *J. Opt. A Pure Appl. Opt.* **5** 183–5

[35] Lindner E, Canning J, Chojetzki C, Brückner S, Becker M, Rothhardt M and Bartelt H 2011 Thermal regenerated type IIa fiber Bragg gratings for ultra-high temperature operation *Opt. Commun.* **284** 183–5

[36] Cook K and Canning J 2008 High-temperature type IIa gratings in 12-ring photonic crystal fibre with germanosilicate core *J. Eur. Opt. Soc. - Rapid Publ.* **3** 08031(1-5)

[37] Lindner E, Canning J, Chojetzki C, Brückner S, Becker M, Rothhardt M and Bartelt H 2011 Post-hydrogen-loaded draw tower fiber Bragg gratings and their thermal regeneration *Appl. Opt.* **50** 2519–22

[38] Bandyopadhyay S, Canning J, Stevenson M and Cook K 2008 Ultrahigh-temperature regenerated gratings in boron-codoped germanosilicate optical fiber using 193 nm *Opt. Lett.* **33** 1917–9

[39] Wang T, Shao L-Y, Canning J and Cook K 2013 Temperature and strain characterization of regenerated gratings *Opt. Lett.* **38** 247–9

[40] Cook K, Smelser C, Canning J, le Garff G, Lancry M and Mihailov S 2012 Regenerated Femtosecond Fibre Bragg

Gratings *Third Asia Pacific Optical Sensors Conference* p 835111
[41] Canning J, Stevenson M, Bandyopadhyay S and Cook K 2008 Extreme Silica Optical Fibre Gratings *Sensors* **8** 6448–52
[42] Åslund M L, Canning J, Fu H and Tam H 2010 Rapid disappearance of regenerated fibre Bragg gratings at temperatures approaching 1500 °C in boron-codoped germanosilicate optical fibre *Fourth European Workshop on Optical Fibre Sensors (EWOFS'10)* p 76530Q
[43] Laffont G, Cotillard R and Ferdinand P 2013 9000 hours-long high temperature annealing of regenerated Fiber Bragg 9000 hours-long high temperature annealing of regenerated Fiber Bragg Gratings *Proc. SPIE 8794, Fifth European Workshop on Optical Fibre Sensors* p 87941X
[44] Chen T, Chen R, Jewart C, Zhang B, Cook K, Canning J and Chen K P 2011 Regenerated gratings in air-hole microstructured fibers for high-temperature pressure sensing *Opt. Lett.* **36** 3542–4
[45] Chen R, Yan A and Chen K P 2014 High-Temperature Flow Sensing Using Regenerated Gratings in Self-Heated High Attenuation Fibers *CLEO:2014, OSA Technical Digest* p paper SF2I.2
[46] Shao L, Canning J, Wang T, Cook K and Tam H-Y 2013 Viscosity of silica optical fibres characterized using regenerated gratings *Acta Mater.* **61** 6071–81
[47] Canning J, Stevenson M and Fenton J 2009 Regenerated gratings *J. Eur. Opt. Soc. - Rapid Publ.* **4** 09052(2-7)
[48] Gao S, Canning J and Cook K 2013 Ultra-high temperature chirped fiber Bragg gratings produced by gradient stretching of viscoelastic silica *Opt. Lett.* **38** 5397–400
[49] Wang T, Shao L, Canning J and Cook K 2013 Regeneration of fiber Bragg gratings under strain *Appl. Opt.* **52** 2080–5
[50] Laffont G, Cotillard R and Ferdinand P 2013 Multiplexed regenerated Fiber Bragg Gratings for high temperature measurement *Meas. Sci. Technol.* **24** 094010
[51] Mihailov S J, Grobnic D, Smelser C W, Walker R B, Lu P and Ding H 2011 Review of femtosecond infrared laser-induced fibre Bragg grating sensors made with a phase mask *Sens. Rev.* **31** 321–7
[52] Martinez A, Dubov M, Khrushchev I and Bennion I 2004 Direct writing of fibre Bragg gratings by femtosecond laser *Electron. Lett.* **40** 1–2
[53] Albert J, Fokine M and Margulis W 2002 Grating formation in pure silica-core fibers *Opt. Lett.* **27** 809–11
[54] Groothoff N, Canning J, Buckley E, Lyttikainen K and Zagari J 2003 Bragg gratings in air-silica structured fibers *Opt. Lett.* **28** 233–5
[55] Lancry M, Poumellec B, Canning J, Cook K, Poulin J-C and Brisset F 2013 Ultrafast nanoporous silica formation driven by femtosecond laser irradiation *Laser Photonics Rev.* **7** 953–62
[56] Lancry M, Poumellec B, Chahid-Erraji A, Beresna M and Kazansky P G 2011 Dependence of the femtosecond laser refractive index change thresholds on the chemical composition of doped-silica glasses *Opt. Mater. Express* **1** 711
[57] Curien L H, Umr C, Lyon U De and Monnet U J 2019 X-ray preconditioning for enhancing refractive index contrast in femtosecond laser photoinscription of embedded waveguides in pure silica *Opt. Mater. Express* **9** 65–74
[58] Grobnic D, Smelser C W, Mihailov S J and Walker R B 2006 Long-term thermal stability tests at 1000 °C of silica fibre Bragg gratings made with ultrafast laser radiation *Meas. Sci. Technol.* **17** 1009–13
[59] Morana A, Girard S, Marin E, Marcandella C, Paillet P, Périsse J, Macé J-R, Boukenter A, Cannas M and Ouerdane Y 2014 Radiation tolerant fiber Bragg gratings for high temperature monitoring at MGy dose levels *Opt. Lett.* **39** 5313–6
[60] Lu J, Yang M, Wang D N, Grattan K T, Sun T and Li Y 2009 Fiber Bragg gratings with enhanced thermal stability by residual stress relaxation *Opt. Express* **17** 19785–90
[61] Robnic D A N G, Natovsky C Y H and Ihailov S T J M 2016 Low loss Type II regenerative Bragg gratings made with ultrafast radiation *Opt. Express* **24** 28704–12
[62] Martinez A, Khrushchev I Y and Bennion I 2005 Thermal properties of fibre Bragg gratings inscribed point-by-point by infrared femtosecond laser *Electron. Lett.* **41** 176–8
[63] Warren-Smith S C, Nguyen L V, Ebendorff-Heidepriem H, Lang C and Monro T M 2016 Temperature sensing up to 1300°C using suspended-core microstructured optical fibers *Opt. Express* **24** 3714–9
[64] ANFF - OptoFab NODE *http://optofab.org.au/uli.html*
[65] Femto Fiber Tec *https://www.femtofibertec.de/de/#home*
[66] Habisreuther T, Elsmann T, Pan Z, Graf A, Willsch R and Schmidt M A 2015 Sapphire fiber Bragg gratings for high temperature and dynamic temperature diagnostics *Appl. Therm. Eng.* **91** 860–5
[67] Busch M, Ecke W, Latka I, Fischer D, Willsch R and Bartelt H 2009 Inscription and characterization of Bragg gratings in single-crystal sapphire optical fibres for high-temperature sensor applications *Meas. Sci. Technol.* **20** 1–6
[68] Elsmann T, Lorenz A, Yazd N S, Habisreuther T, Dellith J, Schwuchow A, Bierlich J, Schuster K, Rothhardt M, Kido L and Bartelt H 2014 High temperature sensing with fiber Bragg gratings in sapphire-derived all-glass optical fibers *Opt. Express* **22** 26825–33
[69] Dragic P, Hawkins T, Foy P, Morris S and Ballato J 2012 Sapphire-derived all-glass optical fibres *Nat. Photonics* **6** 627–33
[70] Grobnic D, Mihailov S J, Ballato J and Dragic P D 2015 Type I and II Bragg gratings made with infrared femtosecond radiation in high and low alumina content aluminosilicate optical fibers *Optica* **2** 313–22
[71] Ballato J and Peacock A C 2018 Perspective: Molten core optical fiber fabrication—A route to new materials and applications *APL Photonics* **3** 120903(1)-120903(14)
[72] Dragic P, Law P-C, Ballato J, Hawkins T and Foy P 2010 Brillouin spectroscopy of YAG-derived optical fibers. *Opt. Express* **18** 10055–67
[73] Sanamyan T, Zhang J, Matthewson M J, Ballato J, Foy P, Daw M, McMillen C, Hawkins T, Kokuoz B, Dubinskii M, Tritt T M, Stolen R and Su Z 2009 On the fabrication of all-glass optical fibers from crystals *J. Appl. Phys.* **105** 053110
[74] Desmarchelier R, Poumellec B, Brisset F, Mazerat S and Lancry M 2015 In the Heart of Femtosecond Laser Induced Nanogratings : From Porous Nanoplanes to Form Birefringence *World J. Nano Sci. Eng.* **5** 115–25
[75] Nesterov A V and Niziev V G 1999 Influence of beam polarization on laser cutting efficiency *J. Phys. D. Appl. Phys.* **32** 1455–61
[76] Kazansky P G, Shimotsuma Y, Sakakura M, Beresna M, Gecevi M, Svirko Y, Akturk S, Qiu J, Miura K and Hirao K 2011 Photosensitivity control of an isotropic medium

through polarization of light pulses with tilted intensity front *Opt. Express* **19** 20657–64
[77] Richter S, Heinrich M, Döring S, Tünnermann A, Nolte S and Peschel U 2012 Nanogratings in fused silica: Formation, control, and applications *J. Laser Appl.* **24** 042008(1)-042008(8)
[78] Markel V A 2016 Introduction to the Maxwell Garnett approximation: tutorial *J. Opt. Soc. Am. A* **33** 1244–56
[79] Bricchi E and Kazansky P G 2006 Extraordinary stability of anisotropic femtosecond direct-written structures embedded in silica glass *Appl. Phys. Lett.* **88** 2–4
[80] Thomson R R, Gillet P, Mukherjee S, Cheng Y, Bellouard Y, Pépin C, McMillen B and Champion A 2016 Stress-state manipulation in fused silica via femtosecond laser irradiation *Optica* **3** 1285
[81] Witcher J J, Reichman W J, Fletcher L B, Troy N W and Krol D M 2013 Thermal annealing of femtosecond laser written structures in silica glass *Opt. Mater. Express* **3** 502–10
[82] Smelser C W, Mihailov S J and Grobnic D 2005 Formation of Type I-IR and Type II-IR gratings with an ultrafast IR laser and a phase mask *Opt. Express* **13** 5377–86